

OPTIMIZATION OF PARAMETERS FOR PRODUCTION OF CARBON NANOFIBERS FROM POLYACRYLONITRILE BY SOLUTION BLOW SPINNING

Lais Angelice de Camargo Gonzaga

National Laboratory of Nanotechnology
Applied to Agribusiness, LNNA, Embrapa
Instrumentation, São Carlos, SP, Brazil
Graduate Program in Chemistry, PPGQ,
UFSCar, São Carlos, SP, Brazil

Pierre-Louis François Henri Personnaz

Department of Materials Science and
Engineering, DEMA, UFSCar, São Carlos, SP,
Brazil
École polytechnique (Polytech Grenoble),
Université Grenoble Alpes, Grenoble, France

Delne Domingos da Silva Parize

National Laboratory of Nanotechnology
Applied to Agribusiness, LNNA, Embrapa
Instrumentation, São Carlos, SP, Brazil
Department of Materials Science and
Engineering, DEMA, UFSCar, São Carlos, SP,
Brazil

Milene Corso Mitsuyuki

National Laboratory of Nanotechnology
Applied to Agribusiness, LNNA, Embrapa
Instrumentation, São Carlos, SP, Brazil

All content in this magazine is
licensed under a Creative Com-
mons Attribution License. Attri-
bution-Non-Commercial-Non-
Derivatives 4.0 International (CC
BY-NC-ND 4.0).



Luiz Henrique Capparelli Mattoso

National Laboratory of Nanotechnology
Applied to Agribusiness, LNNA, Embrapa
Instrumentation, São Carlos, SP, Brazil
Department of Materials Science and
Engineering, DEMA, UFSCar, São
Carlos, SP, Brazil

Abstract: Carbon nanofibers are materials that exhibit a high surface area and good mechanical and thermal properties. For this reason, these fibers are widely used in several areas, such as aircraft and automotive industries. Solution blow spinning (SBS) and electrospinning can be used to produce carbon nanofibers, but SBS is a simpler, cheaper, and effective method to produce micro and nanofibers from polymer solutions. In this work, different SBS conditions were studied to obtain carbon nanofibers using a Box-Behnken experimental design. The physicochemical and thermal properties of the carbon nanofibers were evaluated, as well as their structural properties. The factorial design results indicated that decreasing the PAN mass concentration in solution and increasing the injection rate decreased the nanofiber diameter. After heat treatment, the carbon nanofiber diameter further decreased, ranging from 153.2 (SD: 23.3) with 6% PAN to 369.0 (SD:60.0) with 10% PAN. The carbon nanofibers showed (ID/IG) ratio between 1.17 and 1.20 and crystal size from 16.4 to 16.0 nm for PAN mass concentrations from 6 to 10%, which agrees with the literature. No structural and physico-chemical alterations were observed in the carbon nanofibers, which allows them to be applied in several sectors, such as batteries and capacitors.

Keywords: Carbon nanofibers, Solution blow spinning, Polyacrylonitrile, optimization of production parameters.

INTRODUCTION

Carbon nanofibers display properties of great interest for the market, such as high mechanical strength, low density, high stiffness, and low thermal expansion. These properties make carbon nanofibers important materials for application in the automotive and wind power industries, and especially in batteries, capacitors and supercapacitors [1,

2]. Polyacrylonitrile (PAN) is one of the most used polymers to produce carbon nanofibers. PAN is an atactic and linear polymer made up of 68% carbon and C≡N bonds [1–4]. Carbon nanofibers can be produced using different methods both at exploratory and industrial scales. Electrospinning has been widely studied among them for the production of carbon fibers and nanofibers with diameters between 10 nm and 10 μm from polymeric solutions, as reported in the works of Yan, Liu and Zhang, Arshad, Naraghi, and Chasiotis, Guo and Kim [5–8].

Regarding the production of carbon nanofibers by solution blow spinning (SBS), only a few detailed studies can be found in the literature, such as those reported by Zhuang [9, 10]. SBS is a simple, effective, inexpensive, and safe method that provides a higher fiber production rate compared to electrospinning over a wide range of processing variables [11].

Experimental planning is an approach used to organize and evaluate a set of experiments with the objective of optimizing the process, while describing the influence of each independent variable on an experimental response, including potential cross influences [12].

$$\text{Response variable} = c_5 x^2 + c_4 y^2 + c_3 xy + c_2 x + c_1 y + c_0$$

Box-Behnken planning is a type of factorial planning that is quite suitable to model processes involving many variables. Box-Behnken planning allows to achieve reliable results from a smaller number of experiments when compared to complete experimental designs. For example, if three independent variables are used, the Box-Behnken planning requires 15 experiments, while in a complete planning, 27 experiments would be necessary. Thus, studies are efficiently executed due to the shorter set of experiments, in addition to reduced costs with material, equipments and analysis [12, 13].

In a Box-Behnken planning, each independent variable can assume 3 levels: the minimum, the intermediate (average) and the maximum values, following the practicability of interval. For example, if a process can be feasibly performed using pressure from 1 to 3 bar, the minimum, average and maximum values would be 1, 2 and 3 bar, and these 3 values would be denominated -1, 0 and +1, respectively [14]. The set of experiments generated by the Box-Behnken planning must be carried out randomly to minimize experimental errors effects.

The nanofiber diameter is a factor of great importance, since it depends on the production method and further determines the application of the nanofibers. Nanofibers with small diameters tend to be more suitable for applications in the energy industry, such as capacitors, supercapacitors and batteries [4, 15–20]. Raman spectroscopy, X-ray photoelectron spectroscopy, and elemental analysis, and their electrochemical properties were investigated for the first time as anode in lithium ion batteries (LIBs). To date, the SBS parameters that favor the nanofiber diameter reduction have been little studied. Following this motivation, the present work aimed to study different solution blow spinning (SBS) parameters to produce carbon nanofibers from PAN. A Box-Behnken factorial planning was used to optimize the SBS process towards nanofibers of small diameters

EXPERIMENTAL PROCEDURE

MATERIALS

Polyacrylonitrile (PAN) with $M_w = 150,000$ g/mol was supplied by Sigma-Aldrich Brasil Ltda. (São Paulo, SP, Brazil). N, N-Dimethylformamide (DMF) was obtained from Labsynth Produtos para Laboratórios Ltda. (Diadema, SP, Brazil).

RHEOLOGICAL STUDY OF PAN

PAN solutions in DMF were prepared with mass concentrations from 1% to 12%. These solutions were tested on an Anton Paar Physica rheometer with a concentric cylinder geometry (23.8 and 27.6 mm in diameter and 40 mm in height) in rotational tests. The test temperature was 25 °C. The viscosity was measured from two successive linear tests with shear rates between 1 - 10 s⁻¹ and 10 - 100 s⁻¹ with acquisition time of one second per point.

SOLUTION BLOW SPINNING (SBS)

The SBS system encompassed two nozzles: an internal nozzle through which the polymer solution passes, and an external concentric nozzle through which the pressurized air passes. PAN solutions of various concentrations were prepared and tested in the SBS process. A stirring time of 2 h was used for good PAN solubilization. The experimental conditions were obtained from the Box-Behnken experimental design. The PAN solutions were fed using a 25 mL glass syringe (B – D Yale, Becton – Dickinson & Co, USA) at a rate controlled with an injection syringe pump model NE-1010-US, One Channel 100 lb and a 0.5 mm diameter nozzle. The air pressure was controlled with a pressure regulator. The static collector (shown in Figure 1) was positioned vertically with the surface on rods, allowing the passage of air and the formation of fibers. The temperature was around 28 °C and the relative humidity varied from 35 to 45% throughout the experiments.



FIGURE 1 - Images of the static collector used.

EXPERIMENTAL PLANNING

Three process variables (factors) at three levels were used in the Box-Behnken experimental design: PAN concentration (6, 8 and 10%), injection rate (5.2, 7.2 and 9.2 mL.h⁻¹) and air pressure (1, 2 and 3 bar) (Table 1). The nanofiber diameter was selected as the response variable.

Factors		Levels			
		-1	0	1	
X ₁	PAN concentration	% (wt)	6	8	10
X ₂	Air pressure	bar	1	2	3
X ₃	Injection rate	mL.h ⁻¹	5.2	7.2	9.2

TABLE 1 – Factors and levels of the Box-Behnken factorial design for the production of PAN nanofibers by solution blowing spinning using DMF as a solvent.

The factorial design generated a total of 15 experiments with three repetitions in the central value, which were performed randomly, as shown in Table 2. The PAN concentrations were selected according to the semi-diluted regime from the rheological studies, . Regarding the air pressure and injection rate, the values were selected according to the work of Medeiros and Parize [11, 13]. The levels were determined according to the range between the working limits observed in the previous tests. Beyond these limits PAN nanofibers could not be obtained by SBS.

Pressures lower than those studied in this work did not break the surface tension of the PAN solution, while higher pressures generated high turbulence, preventing attachment of the nanofibers to the collector, in addition to impairing solvent evaporation due to the rapid transport of the solution from the nozzle to the collector. Injection rates lower than those studied here did not allow the formation of nanofibers in the collector, and higher rates promoted the formation of droplets. The average value of $7.2 \text{ mL}\cdot\text{h}^{-1}$ was defined from an earlier report of Oliveira [21].

According to Medeiros and coworkers, the collector distance is also an important factor in the production of nanofibers by SBS [11], because it can also influence on the solvent evaporation. However, in this study, this factor had no significant influence on the response variable and, therefore, was kept constant at 45 cm for all the experiments [9]. This distance is relatively long due to the low evaporation rate of DMF, which requires longer distances for the PAN nanofibers to reach the collector in a dried state.

HEAT TREATMENT

The PAN nanofibers were subjected to stabilization and carbonization treatments. The stabilization step aimed to promote cyclization of the PAN chains to minimize their further degradation in the subsequent treatment. This step was performed in a muffle furnace with a heating ramp of $10 \text{ }^\circ\text{C}\cdot\text{min}^{-1}$ from 25 to $270 \text{ }^\circ\text{C}$. Afterwards, the carbonization step was carried out to eliminate non-carbonic species and enrich the nanofiber microstructure with carbon [22]. This step was performed with a heating ramp of $1 \text{ }^\circ\text{C}\cdot\text{min}^{-1}$ up to $600 \text{ }^\circ\text{C}$ and $3 \text{ }^\circ\text{C}\cdot\text{min}^{-1}$ up to $900 \text{ }^\circ\text{C}$ in a tubular oven under inert atmosphere.

CHARACTERIZATIONS

X-RAY DIFFRACTION (XRD)

Physico-chemical, thermal, and morphological analyses were performed on the PAN and carbon nanofibers. The crystallographic profiles were obtained by X-ray diffraction (DR-X) in a Shimadzu[®]6000 equipment with $\text{CuK}\alpha$ radiation ($\lambda = 1.54 \text{ \AA}$). The operating voltage was 40 kV and the current was 40 mA [23].

FOURIER TRANSFORM INFRARED (FTIR) SPECTROSCOPY

The sample functional groups were identified on an infrared spectrometer Bruker Vertex 70 with Fourier Transform (FTIR) equipped with an attenuated total reflectance accessory (ATR) based on diamond crystal, from 4000 to 400 cm^{-1} with resolution of 4 cm^{-1} and 32 scans per sample.

THERMOGRAVIMETRIC ANALYSIS (TGA)

The thermal stability of the samples was assessed with a TA Instruments[®] equipment, model Q500 (TG / DTG), with sample size of approximately 7-8 mg placed in platinum crucibles. The experiments were carried out with a heating rate of $10 \text{ }^\circ\text{C}\cdot\text{min}^{-1}$ from 25 to $600 \text{ }^\circ\text{C}$ in synthetic air atmosphere with a flow rate of $60 \text{ mL}\cdot\text{min}^{-1}$. From the TG/DTG curves, the following parameters were obtained: volatility ($\% \text{ H}_2\text{O}$) which is estimated as the mass loss at $150 \text{ }^\circ\text{C}$, and T_{onset} (the onset of degradation), which was obtained by the tangent method

RAMAN SPECTROSCOPY

Raman spectroscopy was carried out on a Horman Scientific[®] model LabRAM HR Evolution Raman spectrometer equipped with a Czerny-Turner monochromator, CCD detector and an Olympus confocal

microscope (50x objective lens) with laser: 532. The laser power on the sample surface was approximately 1 mW to avoid possible degradation effects. From the band intensity ratio and laser wavelength, the crystallite size was estimated from Equation 1 [24]

$$\text{Crystal size (nm)} = \frac{2.4 \times 10^{-10} \times \lambda^4}{ID/IG} \quad (\text{Equation 1})$$

SCANNING ELECTRON MICROSCOPY (SEM)

The fiber morphology was examined by scanning electron microscopy (SEM), using a JEOL[®] JSM-6701F microscope equipped with a field emission gun and running at 10 kV. A small portion of each sample was deposited onto a carbon tape, and further coated with a thin gold layer (~15 nm).

RESULTS AND DISCUSSION

The PAN concentration range used in the factorial planning was first defined through a series of rheological profiles obtained for PAN solutions with different mass concentrations (Figure 2).

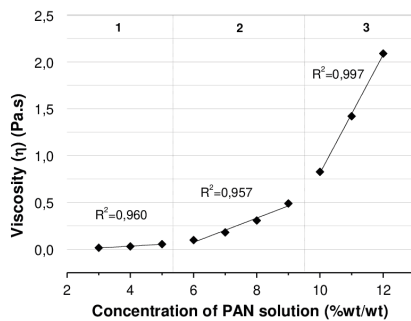


FIGURE 2 - Viscosity (η) as a function of PAN solution concentration in DMF (fixed shear rate of 100 s^{-1} at 25°C).

Figure 3 shows the relationship between the solution viscosity and PAN concentration. The solution viscosity was proportional to the PAN concentration, and different regimes are observed.

At low mass concentrations, from 3 to 5%,

the solutions are in the diluted regime, whereas from 6 to 9% and 10 to 13%, the solutions are in the semi-diluted and concentrated regimes, respectively. The concentration range used in the SBS process is that of the semi-diluted regime, that is, PAN concentrations between 6 and 9%. The semi-diluted regime is normally used in the production of nanofibers by SBS due to the optimized viscoelastic solution properties with a polymer/solvent ratio high enough to allow the entanglement between the polymer chains [25].

The concentrated regime regularly causes the needle to clog, and, consequently, interrupts the production of nanofibers. Yet the diluted regime, the solution does not have enough viscoelasticity to form nanofibers in the collector due to the small amount of polymer in solution.

Figure 3 shows the flow behavior of the PAN solutions at different mass concentrations under different shear rates ($1-100 \text{ s}^{-1}$).

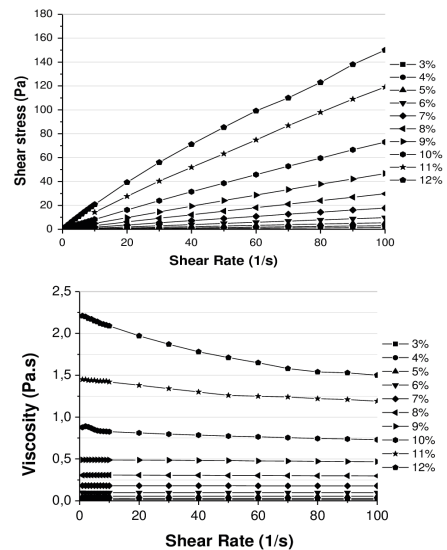


FIGURE 3 – Viscosity (η) and Shear Stress (Pa) of PAN solutions (w/w) when subjected to a fixed shear rate of 100 s^{-1} a 25°C

According to the data presented in Figure 3, it can be seen that the PAN solution has a viscosity independent on the shear rate for the lowest mass concentrations. For the highest PAN concentrations, a decrease in viscosity

Order of experiments		PAN mass concentration	Air pressure (bar)	Injection rate (mL/Hr)	Average diameter (nm)	Median diameter (nm)	Standard deviation (nm)
Standard	Random						
1	1	6	2	7,2	457	449	121
2	5	6	3	5,2	434	429	107
3	4	10	4	7,2	700	714	116
4	14	8	3	7,2	569	542	125
5	9	8	2	5,2	603	593	140
6	17	8	3	7,2	526	520	130
7	13	8	3	7,2	508	543	160
8	16	8	3	7,2	550	538	131
9	8	10	3	9,2	610	608	99
10	6	10	3	5,2	521	509	152
11	15	8	3	7,2	706	720	137
12	3	6	4	7,2	294	292	60
13	12	8	4	9,2	358	355	73
14	7	6	3	9,2	322	314	72
15	11	8	2	9,2	309	277	125
16	2	10	2	7,2	885	884	216
17	10	8	4	5,2	435	438	137

TABLE 2 - Factorial design matrix: average diameter, median diameter and standard deviation of PAN fibers obtained by solution blow spinning using DMF as a solvent.

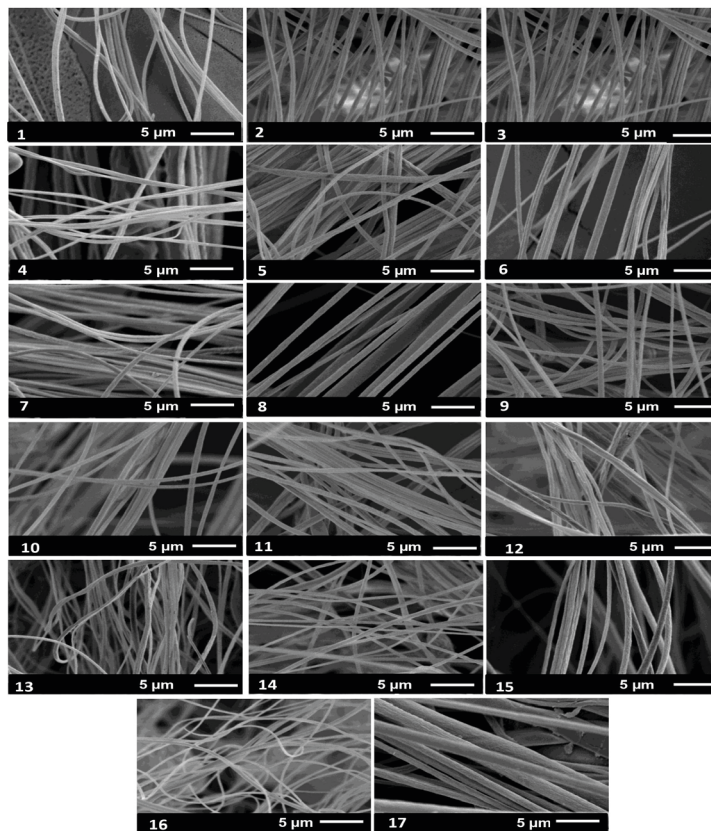


FIGURE 4 - SEM micrographs of PAN nanofibers obtained by SBS using DMF as a solvent according to the BBD factorial planning (standard order).

occurs with increasing the shear rate.

Therefore, at high concentrations, approximately 10 - 12%, the solutions present a pseudoplastic behavior, proving that in this region the viscosity would be affected by the shear forces in the SBS process.

The Box-Behnken factorial design (Table 1) was carried out in the semi-diluted regime to evaluate the effect of three SBS parameters at three levels on the PAN nanofiber diameter. Table 2 shows the results of each experiment obtained from the SEM micrographs shown in Figure 4.

From Table 2, it is possible to notice different ranges of average diameters among the experiments using different PAN concentrations. The average diameters of the PAN nanofibers with mass concentration of 6% were from 294 to 457 nm, from 309 to 610 nm for 8% and from 521 to 885 nm for 10%. These results indicate that the PAN concentration plays a key role in determining the nanofiber diameter.

The micrographs reveal homogeneous nanofibers in all the experiments with little formation of granules or drops. Some fibers appear interconnected, indicating that the DMF was not fully evaporated even using the 45 cm working distance between the nozzle and collector. The distance of 45 cm is close to the optimal distance found in another work on SBS of PAN nanofibers by Zhuang [9]. The use of longer distances causes the nanofibers to deviate along the path without reaching the collector [25].

Figure 5 shows the box chart for each BBD factorial design experiment.

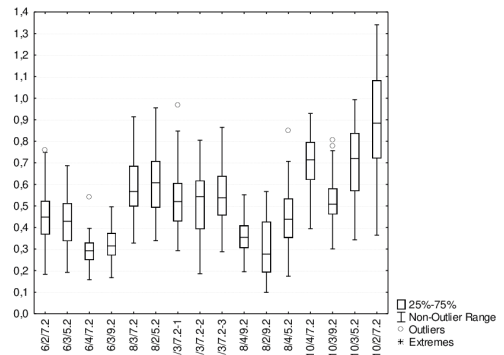


FIGURE 5 - Box plot of PAN nanofiber diameters obtained by SBS using DMF as a solvent from the BBD factorial design of experiments (standard order). The horizontal lines in the middle of each box show the median values. The box margins represent 25% and 75% points and the outer bars correspond to the maximum and minimum values obtained.

As previously mentioned, the SBS process often generates a broad diameter distribution curve, which increases the standard deviation, affecting the statistical analysis. Therefore, the median was used as the response variable as an alternative to achieve a better model fit, as the median is not affected by the extreme values of the diameter distribution curve [13].

Figure 6 shows the response surface graphs of the PAN nanofiber diameter median as a function of the polymer concentration and injection rate.

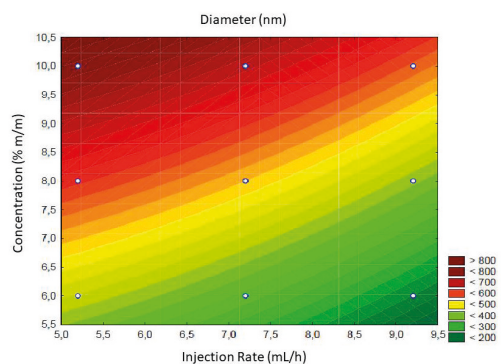


FIGURE 6 - Response surface plot showing the nanofiber diameter as a function of injection rate and PAN concentration.

It is possible to observe the relationship

between the experimental factors and nanofiber diameters. In Figure 6, the color variations indicate that decreasing the PAN concentration reduced the nanofiber diameter. Similar results have been reported previously in the literature by Zhuang [9], for the production of PAN nanofibers by SBS, and Parize [25], for the obtaining of PLA nanofibers by SBS using a chloroform/acetone mixture as a solvent.

The influence of the PAN concentration, air pressure and injection rate on the PAN nanofiber production by SBS using DMF was described by the quadratic model (Equation 2) obtained by analysis of variance (ANOVA) using only the significant effects [26].

$$y = \beta_0 + \sum \beta_i x_i k_i = 1 + \sum \beta_{ii} x_{i2} k_i = 1 + \sum \beta_{ij} x_i x_j k_i < j = 2 + \varepsilon \quad (\text{Equation 2})$$

Where y is the response variable, β are the model regression coefficients, x are the independent variables and ε is the random error component. The model's errors were assumed to be a random variable independently distributed, with zero mean value and constant variance σ^2 .

ANOVA showed that the linear and quadratic coefficients of mass concentration, the quadratic coefficient of the injection rate and all linear interactions were significant ($p = 0.05$) on the PAN nanofiber diameter. Unlike these two factors, the air pressure did not have a direct effect on the diameters, in opposition to the results from Zhuang [9] for the production of PAN nanofibers by SBS. According to the author, the higher the air pressure, the smaller the nanofiber diameter, but this conclusion was not based on statistical analyses.

Therefore, in this study, the model was described as a reduced equation considering only the significant coefficients, where the PAN concentration and injection rate were coded as X_1 and X_2 , respectively (Equation 3).

The determination coefficient (R^2) was 0.88, indicating that more than 88% of the results can be explained by the model.

$$\hat{y} = 429 + 336[X_1] + 195[X_2]^2 \quad (\text{Equation 3})$$

The nanofiber samples obtained from the solutions with PAN mass concentration of 6, 8 and 10% were characterized by FTIR and XRD. Figures 7 and 8 show the results for the sample related to the concentration of 8%, as no differences were observed in relation to the other samples.

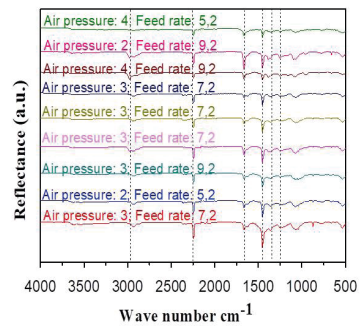


FIGURE 7 – FTIR spectra of PAN nanofibers obtained from the 8% PAN mass concentration in DMF using different air pressures and injection rates

The FTIR spectrum in Figure 7 shows reflectance bands related to the PAN groups. The nanofibers showed bands ranging from 2241 to 2243 cm^{-1} related to the $\text{C}\equiv\text{N}$ bonds [27]. The bands corresponding to PAN aliphatic groups are present at around 2800, 1400, 1300 and 1200 cm^{-1} [28].

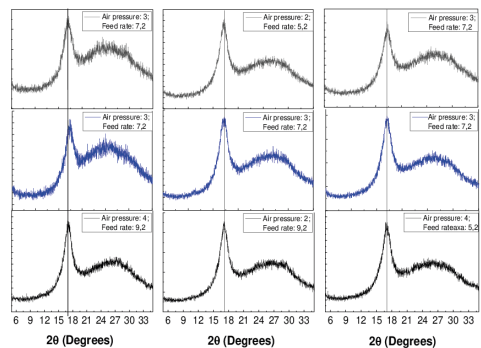


FIGURE 8 – X-ray diffractogram of PAN nanofibers obtained from the 8% PAN mass concentration in DMF using different air pressures and injection rates.

The samples presented an intense peak at 17° of 2θ , and a less intense and broader peak at 29° of 2θ , which are characteristic of the planes (100) and (101), respectively, of PAN chains [29, 30].

All the samples presented FTIR and XRD patterns similar to those found in the literature for PAN powder and PAN nanofibers produced by electrospinning using different mass concentrations. This shows that the SBS process did not change the physicochemical properties of the nanofibers.

The nanofibers were also analyzed via TGA, as represented by nanofibers with a mass concentration of 8% in Figure 9.

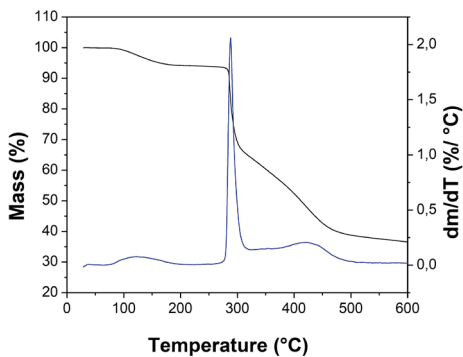


FIGURE 9 - TG/DTG curves of PAN nanofibers obtained from the 8% PAN mass concentration in DMF

The PAN nanofibers were stable up to 280°C , with a maximum degradation temperature (T_{max}) of around 283.7°C . According to Rahaman [22], the thermal profile of PAN presents well-defined temperatures and reactions. At temperatures above 250°C , PAN undergoes cyclization reactions, increasing the rigidity of the polymer chain. Subsequently, dehydrogenation occurs in two steps, oxidation, and water elimination, and finally the polymer suffers oxidation, providing greater stability to the fiber for the subsequent steps.

Table 3 shows the thermal analysis results of the PAN nanofibers with a mass concentration

of 8%.

% Volatility	Tonset ($^\circ\text{C}$)	Tmax ($^\circ\text{C}$)	% Residue	R ($\%/^\circ\text{C}$)
0.42	277.3	283.7	39.6	3.0

TABLE 3 - Thermal properties of PAN nanofibers with 8% physical concentration.

The PAN nanofibers showed a continuous mass loss with a rate of $3.0\%/^\circ\text{C}$. The second most evident degradation occurred at around 410°C , similar to that found in the literature for PAN nanofibers produced by electrospinning [27].

Carbon nanofibers were obtained after thermal treatment (stabilization and carbonization) of PAN nanofibers. Figure 10 shows the PAN morphological changes throughout the whole process, from SBS to the carbon nanofiber state.

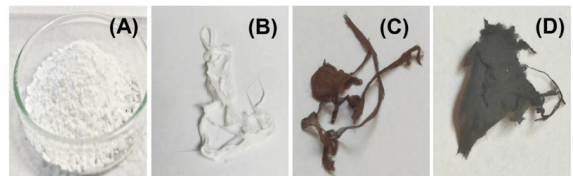


FIGURE 10 - Images of (A) PAN and PAN nanofibers (B) After SBS (C) Stabilization (D) Carbonization

The PAN nanofibers exhibit a white color due to the polymer. After stabilization, the nanofibers acquire a light brown coloration, and after carbonization the darker color typical of carbon materials is noticeable.

Figure 11 shows the SEM micrographs of the PAN nanofibers obtained from three concentrations and their resulting carbon nanofibers.

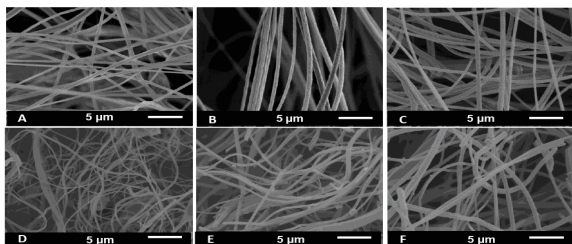


FIGURE 11 – SEM micrographs of PAN nanofibers with mass concentration of (a, b, c) - 6, 8 and 10% and carbon nanofibers with mass concentration of (d, e, f) - 6, 8 and 10%.

From Figure 11, it is noticed that the thermal treatment may have induced the rupture of the carbon nanofibers, as loose fiber ends are observed, but not in the PAN nanofibers before the carbonization process (Figure 2).

This rupture is most likely due to the evaporation of the main non-carbonic components of the nanofibers, causing a contraction and reduction in the CNF diameter [31]. The diameters measured for the precursor PAN nanofibers, stabilized nanofibers and CNF are presented in Figure 12.

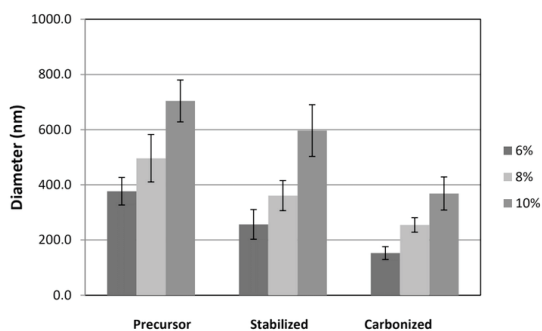


FIGURE 12 – Mean diameter and standard deviation of PAN nanofibers obtained by SBS using DMF and mass concentrations of 6, 8 and 10%, before and after the stabilization and carbonization processes.

The nanofibers diameter increased with increasing the PAN concentration, which may be linked to the higher solution viscosities [1,

32]. After thermal treatment, the nanofiber diameter decreased by around 40 - 50%, presenting an average value of 153.2 (SD:23.3), 254.0 (SD:26.3) and 369.0 (SD:60.0) for the PAN mass concentrations of 6, 8 and 10%, respectively. This reduction occurs due to the formation of cyclic structure and volatilization of some non-carbonic components during the process, such as nitrogen, hydrogen and oxygen, among others [1, 32]. The carbon nanofibers were also evaluated by Raman and XRD (Figure 13).

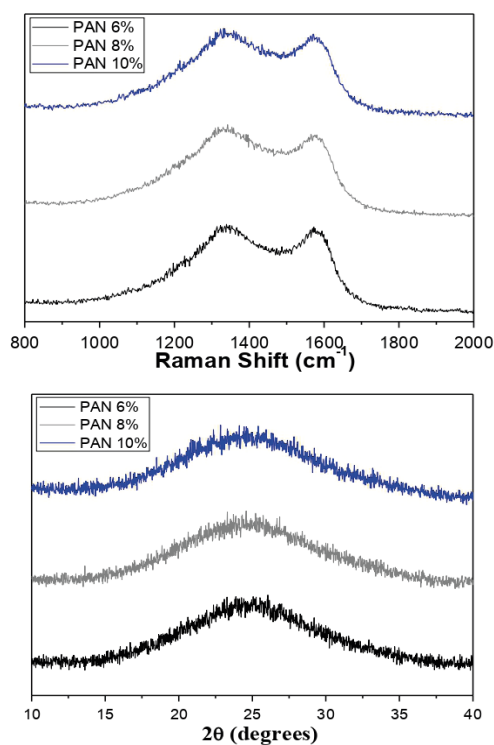


FIGURE 13 – Raman and XRD patterns of carbon nanofibers from PAN mass concentrations of 6, 8 and 10%.

The Raman spectrum show two characteristic bands of carbonic structures. These bands at 1320 and 1580 cm^{-1} are related to the so-called D-band and G-band, respectively. The D-band is related to the disordered carbon vibration mode [33], whereas the G-band relates to all C = C bond vibration modes of sp^2 hybridized carbons in

graphical structures [15, 28, 31, 33].

The analysis of the ID/IG ratio (R), was carried out from the Lorentzian lines, using the software Origin 8.0 to collect the intensity of the D- and G-bands that indicates the disorder degree in carbon-based materials, and enables the crystallite size to be estimated by Equation 1, as presented in the experimental procedure [15, 24]”ISBN”:.”0141-8130””;abstract”:.”The graft copolymerization of acrylonitrile (AN. Table 4 shows the (ID/IG) ratio and the crystal size in nm for the PAN carbon nanofibers with mass concentrations of 6, 8 and 10%.

	6%	8%	10%
R (ID/IG)	1.17	1.25	1.20
Crystal size (nm)	16.4	15.4	16.0

TABLE 4 – ID/IG ratio (R) and crystal size in nm obtained by Raman analysis at 532 nm for PAN carbon nanofibers with different mass concentrations obtained by SBS.

The wavelength (λ) used in the equation was 532 nm. As can be seen in Table 4, the ID/IG ratios were close to 1.20, in agreement with the values found in the literature for PAN nanofibers with a carbonization temperature of 1000 °C [24, 34, 35].

It is possible to notice in the XRD pattern a peak close between 20 - 30° of 2θ . This is associated with the crystallographic plane (002) of graphitic compounds, as also observed by Abeykoon, Kim and Zhao [5, 34, 35].

CONCLUSIONS

The factorial planning was proved to be efficient for optimizing the experimental conditions of the carbon nanofiber production by SBS. The median response was used to evaluate the data obtained through the planning due to the number of outliers generated in the SBS experiments, enabling a better model fitting. The results showed that the lower the concentration and the higher the injection rate used in the SBS, the smaller the nanofiber diameter. The pressure did not play a key role on the PAN nanofiber diameters, thus being disregarded in the final model. The carbon nanofibers presented diameters from 153.2 to 369.0 nm for PAN mass concentrations from 6 to 10% respectively, corroborating with the results found in the factorial design. These nanofibers showed characteristic Raman bands of graphitic compounds, with ID/IG ratios, crystal sizes and diameter similar to the values found in the literature for nanofibers carbonized at 1000 °C. Thus, it was possible to produce PAN-based carbon nanofibers with small diameters by SBS, a product that has a high added-value in the market.

ACKNOWLEDGMENTS

The authors thank Coordination for the Improvement of Higher Education Personnel (CAPES), National Council for Scientific and Technological Development (CNPq), National System of Nanotechnology Laboratories (SISNANO) and Rede AgroNano (Brazil) for the financial support.

COMPLIANCE WITH ETHICAL STANDARDS

Conflict of Interest: The authors declare that they have no conflict of interest.

REFERENCES

1. Huang X (2009) Fabrication and properties of carbon fibers. *Materials (Basel)* 2:2369–2403. <https://doi.org/10.3390/ma2042369>
2. Frank E, Hermanutz F, Buchmeiser MR (2012) Carbon fibers: Precursors, manufacturing, and properties. *Macromol Mater Eng* 297:493–501. <https://doi.org/10.1002/mame.201100406>
3. Shin HK, Park M, Kim HY, Park SJ (2015) An overview of new oxidation methods for polyacrylonitrile-based carbon fibers. *Carbon Lett* 16:11–18. <https://doi.org/10.5714/CL.2015.16.1.011>
4. Wang X, Zhang W, Chen M, Zhou X (2018) Electrospun enzymatic hydrolysis lignin-based carbon nanofibers as binder-free supercapacitor electrodes with high performance. *Polymers (Basel)* 10:. <https://doi.org/10.3390/polym10121306>
5. Kim C, Jeong Y Il, Ngoc BTN, et al (2007) Synthesis and characterization of porous carbon nanofibers with hollow cores through the thermal treatment of electrospun copolymeric nanofiber webs. *Small* 3:91–95. <https://doi.org/10.1002/sml.200600243>
6. Arshad SN, Naraghi M, Chasiotis I (2011) Strong carbon nanofibers from electrospun polyacrylonitrile. *Carbon N Y* 49:1710–1719. <https://doi.org/10.1016/j.carbon.2010.12.056>
7. Guo L, Bai J, Wang J, et al (2015) Fabricating series of controllable-porosity carbon nanofibers-based palladium nanoparticles catalyst with enhanced performances and reusability. *J Mol Catal A Chem* 400:95–103. <https://doi.org/10.1016/j.molcata.2015.02.009>
8. Yan H, Liu L, Zhang Z (2011) Continually fabricating staple yarns with aligned electrospun polyacrylonitrile nanofibers. *Mater Lett* 65:2419–2421. <https://doi.org/10.1016/j.matlet.2011.04.091>
9. Zhuang XP, Jia KF, Cheng BW, et al (2013) Preparation of Polyacrylonitrile Nanofibers by Solution Blowing Process. *J Eng Fiber Fabr* 8:88–93
10. Zhuang XP, Jia KF, Cheng BW, et al (2014) Solution blowing of continuous carbon nanofiber yarn and its electrochemical performance for supercapacitors. *Chem Eng J* 237:308–311. <https://doi.org/10.1016/j.cej.2013.10.038>
11. Medeiros ES, Glenn GM, Klamczynski AP, et al (2009) Solution blow spinning: A new method to produce micro- and nanofibers from polymer solutions. *J Appl Polym Sci* 113:2322–2330. <https://doi.org/10.1002/app.30275>
12. Box GE, Behnken DW (1960) Some New Three Level Designs for the Study of Quantitative Variables. *Technometrics* 2:455–475. <https://doi.org/http://dx.doi.org/10.1080/00401706.1960.10489912>
13. da Silva Parize DD, Foschini MM, de Oliveira JE, et al (2016) Solution blow spinning: Parameters optimization and effects on the properties of nanofibers from poly(lactic acid)/dimethyl carbonate solutions. *J Mater Sci* 51:4627–4638. <https://doi.org/10.1007/s10853-016-9778-x>
14. Ferreira SLC, Bruns RE, Ferreira HS, et al (2007) Box-Behnken design: An alternative for the optimization of analytical methods. *Anal Chim Acta* 597:179–186. <https://doi.org/10.1016/j.aca.2007.07.011>
15. Wang SX, Yang LP, Stubbs LP, et al (2013) Lignin-Derived Fused Electrospun Carbon Fibrous Mats as High Performance Anode Materials for Lithium Ion Batteries. *ACS Appl Mater Interfaces* 5:12275–12282. <https://doi.org/10.1021/am4043867>
16. Norberg I, Nordstrom Y, Drougge R, et al (2013) A new method for stabilizing softwood kraft lignin fibers for carbon fiber production. *J Appl Polym Sci* 128:3824–3830. <https://doi.org/10.1002/app.38588>
17. Lai C, Zhou Z, Zhang L, et al (2014) Free-standing and mechanically flexible mats consisting of electrospun carbon nanofibers made from a natural product of alkali lignin as binder-free electrodes for high-performance supercapacitors. *J Power Sources* 247:134–141. <https://doi.org/10.1016/j.jpowsour.2013.08.082>

18. Schlee P, Herou S, Jervis R, et al (2019) Free-standing supercapacitors from Kraft lignin nanofibers with remarkable volumetric energy density. *Chem Sci* 10:2980–2988. <https://doi.org/10.1039/c8sc04936j>
19. Ma X, Smirnova AL, Fong H (2019) Flexible lignin-derived carbon nanofiber substrates functionalized with iron (III) oxide nanoparticles as lithium-ion battery anodes. *Mater Sci Eng B Solid-State Mater Adv Technol* 241:100–104. <https://doi.org/10.1016/j.mseb.2019.02.013>
20. Tao L, Huang Y, Zheng Y, et al (2019) Porous carbon nanofiber derived from a waste biomass as anode material in lithium-ion batteries. *J Taiwan Inst Chem Eng* 95:217–226. <https://doi.org/10.1016/j.jtice.2018.07.005>
21. Oliveira J, Brichi GS, Marconcini JM, et al (2014) Effect of solvent on the physical and morphological properties of poly(lactic acid) nanofibers obtained by solution blow spinning. *J Eng Fiber Fabr* 9:117–125. <https://doi.org/10.1177/155892501400900414>
22. Rahaman MSA, Ismail AF, Mustafa A (2007) A review of heat treatment on polyacrylonitrile fiber. *Polym Degrad Stab* 92:1421–1432. <https://doi.org/10.1016/j.polymdegradstab.2007.03.023>
23. Facchinatto WM, Fiamingo A, dos Santos DM, Campana-Filho SP (2019) Characterization and physical-chemistry of methoxypoly(ethylene glycol)-g-chitosan. *Int J Biol Macromol* 124:828–837. <https://doi.org/10.1016/j.ijbiomac.2018.11.246>
24. Youe WJ, Lee SM, Lee SS, et al (2016) Characterization of carbon nanofiber mats produced from electrospun lignin-g-polyacrylonitrile copolymer. *Int J Biol Macromol* 82:497–504. <https://doi.org/10.1016/j.ijbiomac.2015.10.022>
25. Da Silva Parize DD, De Oliveira JE, Foschini MM, et al (2016) Poly(lactic acid) fibers obtained by solution blow spinning: Effect of a greener solvent on the fiber diameter. *J Appl Polym Sci* 133:1–10. <https://doi.org/10.1002/app.43379>
26. Montgomery DC (1984) Design and analysis of experiments
27. Oroumei A, Fox B, Naebe M (2015) Thermal and Rheological Characteristics of Biobased Carbon Fiber Precursor Derived from Low Molecular Weight Organosolv Lignin. *ACS Sustain Chem Eng* 3:758–769. <https://doi.org/10.1021/acssuschemeng.5b00097>
28. Choi DI, Lee JN, Song J, et al (2013) Fabrication of polyacrylonitrile/lignin-based carbon nanofibers for high-power lithium ion battery anodes. *J Solid State Electrochem* 17:2471–2475. <https://doi.org/10.1007/s10008-013-2112-5>
29. Dong XG, Wang CG, Chen J, Cao WW (2008) Crystallinity development in polyacrylonitrile nascent fibers during coagulation. *J Polym Res* 15:125–130. <https://doi.org/10.1007/s10965-007-9151-5>
30. Sánchez-Soto PJ, Avilés MA, Del Río JC, et al (2001) Thermal study of the effect of several solvents on polymerization of acrylonitrile and their subsequent pyrolysis. *J Anal Appl Pyrolysis* 58–59:155–172. [https://doi.org/10.1016/S0165-2370\(00\)00203-5](https://doi.org/10.1016/S0165-2370(00)00203-5)
31. Ma A, Zhou L, Chang J (2015) Conversion of lignin-nanofibers to CNFs. *Nano* 10:1–9. <https://doi.org/10.1142/S1793292015500927>
32. Cho M, Ko FK, Rennecker S (2019) Impact of Thermal Oxidative Stabilization on the Performance of Lignin-Based Carbon Nanofiber Mats. *ACS Omega* 4:5345–5355. <https://doi.org/10.1021/acsomega.9b00278>
33. Höfelmann KCG (2013) Espectroscopia Raman por Transformada de Fourier e análise de molhabilidade nos filmes finos de carbono amorfo hidrogenado (a-C:H). 68
34. Abeykoon NC, Mahmood SF, Yang DJ, Ferraris JP (2019) Electrospun poly(acrylonitrile-co-itaconic acid) as a porous carbon precursor for high performance supercapacitor: Study of the porosity induced by in situ porogen activity of itaconic acid. *Nanotechnology* 30. <https://doi.org/10.1088/1361-6528/ab32c0>
35. Zhao X, Nie G, Luan Y, et al (2019) Nitrogen-doped carbon networks derived from the electrospun polyacrylonitrile@branched polyethylenimine nanofibers as flexible supercapacitor electrodes. *J Alloys Compd* 808:151737. <https://doi.org/10.1016/j.jallcom.2019.151737>